IEEE Access
Multidisciplinary ⋮ Rapid Review ⋮ Open Access Journal

Received 20 December 2024, accepted 5 January 2025, date of publication 8 January 2025, date of current version 14 January 2025.

*Digital Object Identifier 10.1109/ACCESS.2025.3526970*

RESEARCH ARTICLE

# Investigating the Formation of Trace Metal Contamination in Insulating Oil: From Electrical Erosion and Chemical Corrosion Perspectives

**FENG WANG[1,2], (Senior Member, IEEE), HUIMIN ZHANG[1], HAOCHENG WANG[1], DILIXIATI HAYIREDING[1], CANGUAN GAO[1], GUOLIANG ZHANG[1], KAIBIN LIANG[2], HENG YI[2], ZEPING HUANG[2], AND CHANGHAO HU[2]**

[1]Department of Electronics and Engineering, Yili Normal University, Gulja, Yining 835000, China
[2]College of Electrical and Information Engineering, Hunan University, Changsha 410082, China

Corresponding author: Kaibin Liang (liangkb@hnu.edu.cn)

This work was supported by the National Natural Science Foundation of China under Grant 52237007 and Grant 52407171.

**ABSTRACT** The presence of trace metal in transformer oil significantly affects its insulating properties, posing potential risks to the safe operation of transformers. Therefore, understanding the intrinsic mechanisms behind the formation of the trace copper within transformers is of critical importance. In this study, we investigated the two primary forms of trace copper in transformer oil—suspended particulate and soluble ionic states—and conducted detailed experimental analyses to elucidate their formation mechanisms. Through electrical arcing experiments, we examined the behavior of metal contacts in insulating oil, identifying the transfer of surface material during arc interruption as a crucial pathway for the generation of suspended metallic particulates. Additionally, we explored the impact of electrical arcing on the damage mechanisms of the contacts and the resulting microstructural characteristics of the ablated surfaces. Corrosion tests were employed to study the formation mechanisms of metal ions, with both macroscopic and microscopic analyses performed on different corrosion morphologies. Our findings suggest the presence of copper corrosion products and their soluble forms, specifically identifying copper-oleate as a major component, which demonstrates high solubility and diffusion capacity in the oil.

**INDEX TERMS** Insulating oil, metal contamination, arc ablation, chemical corrosion, soluble copper.

## I. INTRODUCTION

Large power transformers, as one of the most critical components of the power grid, play a vital role in ensuring the safe and reliable operation of the entire electrical network. A statistical investigation conducted by the International Council on Large HV Electric Systems (CIGRE) on 964 transformer failures (with voltage ratings ≥60 kV) indicates that insulation failures due to dielectric degradation are the primary cause of internal transformer faults, as illustrated in Figure 1 [1], [2]. In transformers, the dielectric primarily refers to mineral insulating oil, which often faces quality degradation over prolonged operational periods. Various factors contribute to the deterioration of insulating oil, including the presence of trace moisture, dissolved gases, fiber contamination, and metallic pollutants. Previous research by scholars and institutions has extensively explored the mechanisms and impacts of dissolved moisture, gases, and fiber contamination in oil, leading to a clearer understanding of these phenomena [3], [4], [5]. However, the sources of metallic contamination remain less well-defined. It is generally believed that such metallic debris arises from external factors during the manufacturing, transportation, and installation processes, or from the dissolution of metal ions in internal anti-corrosion coatings, leading to the contamination of insulating oil. Nonetheless, there is limited research addressing the processes by which metallic particles may originate intrinsically within the transformer.

The associate editor coordinating the review of this manuscript and approving it for publication was Yuh-Shyan Hwang.

The presence of trace metals significantly impacts the insulating properties of transformer oil [6], [7]. For instance, copper and iron particulates, which are commonly found in transformers, not only reduce the breakdown voltage of the oil but also accelerate its oxidative aging process. The formation of these metal particles is often associated with the phenomenon of electrical erosion. However, current research on the electrical erosion behavior of metal materials predominantly occurs in vacuum or insulating gas environments, with limited investigation into their behavior within insulating oil. Therefore, it is imperative to explore the effects of electrical erosion processes on contact points, as well as to examine the mechanisms underlying the generation of metallic particulates during electrical erosion and the factors influencing this process.

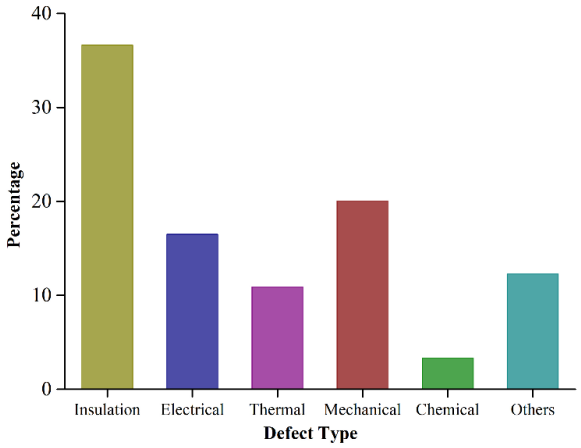


**FIGURE 1.** Transformer failure mode analysis based on 964 major failures.

The presence of metals in transformer oil manifests not only as visible suspended particulate matter but also as soluble metal ionic compounds [6]. These metal ions can significantly alter the dielectric properties of insulating oil; however, their subtle presence often goes unnoticed. The persistent inability to further reduce dielectric losses in recycled oil post-filtration can be attributed to the presence of these non-filterable soluble metal ions. Currently, there is a notable gap in the understanding of the formation mechanisms of soluble metal ions in oil, as well as their impact on the electrical performance of insulating oil. Experimental evidence indicates that the presence of metal ions adversely affects the electrical properties of insulating oil, underscoring the necessity for in-depth mechanistic studies in this area.

Based on the current state of knowledge, this study primarily investigates the electro-erosion process of metals in oil and its influencing factors, which is integral to the formation of endogenous metallic particles within transformers. Subsequently, the research examines the corrosive behavior of typical corrosive sulfides (DBDS) and acids (formic acid, oleic acid) on contact materials, revealing a significant presence of insoluble metal sulfides and soluble metal ionic compounds among the corrosion products. This work elucidates the mechanisms underlying the formation of both suspended and soluble trace metals in transformers, providing critical insights for the prevention of metallic contamination in insulating oils.

## II. ARC ABLATION PROCESS OF METAL ELECTRODES IN OIL

### A. EXPERIMENTAL METHOD AND PLATFORM

When investigating the electrical ablation characteristics of contact materials, a needle-plate electrode configuration can be employed [8], [9], [10]. By adjusting the voltage, a continuous low-current arc is generated between the electrodes, allowing for the examination of the effects of electrical ablation on the contact surfaces. The testing circuit designed to simulate the electrical ablation of metal contacts is illustrated in Figure 2. During the testing process, the liquid within the entire testing unit is maintained at a specific height, ensuring that the electrode gap is submerged in the insulating oil, with a total volume of approximately 1.5 liters of insulating oil within the testing unit.

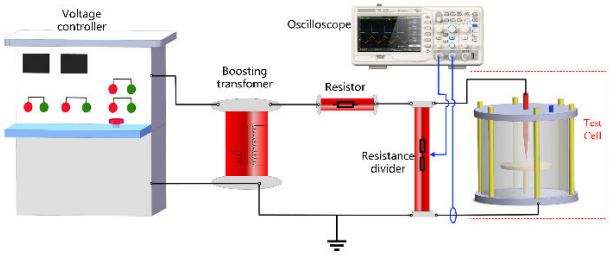


**FIGURE 2.** Schematic diagram of the contact ablation testing platform.

During the experimental procedure, the oil gap of the needle-plate electrode was set to 10 mm, allowing for the maintenance of an electric arc at a relatively low voltage (with an applied voltage of 20 kV in this study). At this setting, the heat generated by the current-limiting resistor remained within acceptable limits. To investigate the effects of sustained electrical ablation on the cathode material, we examined the changes in the microstructure of samples at various time intervals, thereby elucidating the arc ablation process. The cathode samples consisted of 0.05 mm thick copper or silver plates placed on the surface.

The surface morphology of electrode materials undergoes significant alterations following arc erosion. Figure 3 illustrates the erosion patterns of the copper cathode at various time intervals as observed under an optical microscope. Initially, the application of arc current leads to the formation of irregular micro-pits on the cathode surface, culminating in the development of a circular erosion pit at the core of the arc. Notably, the cathode specimen is perforated within four minutes. In contrast, Figure 4 presents the erosion characteristics of the silver cathode. Similar to the copper cathode, the initial response to arc current results in the emergence of numerous micro-pits on the surface, which progressively coalesce into a central erosion cavity, with complete perforation occurring within five minutes.

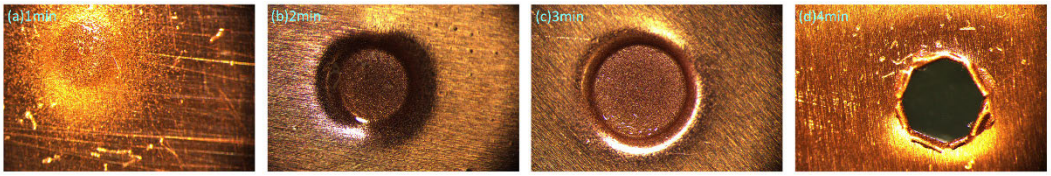


**FIGURE 3.** Cathodic metal ablation conditions at different time under optical microscope (copper).

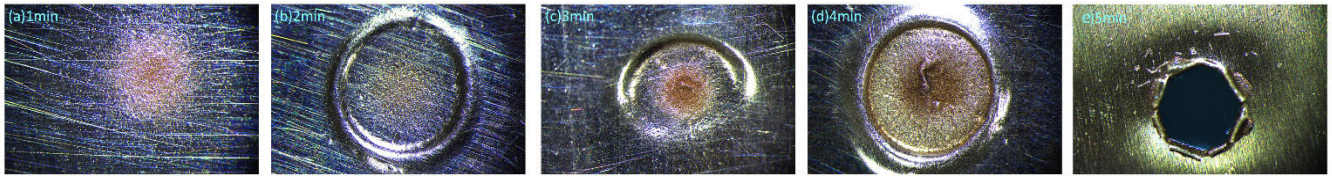


**FIGURE 4.** Cathodic metal ablation conditions at different time under optical microscope (silver).

Throughout the erosion process, despite the continuity of the current pathway, the arc current remains unstable, and discharges between the oil gaps occur with abnormal frequency. It is noteworthy that multiple identical metal samples were subjected to erosion experiments for durations of 1, 2, 3, 4, and 5 minutes, ensuring a comprehensive analysis of the erosion dynamics.

The schematic representation of the discharge circuit is illustrated in Figure 5, where the oil gap is modeled as a nonlinear impedance. Additionally, the effects of stray capacitance and ground capacitance are incorporated, represented by an equivalent capacitance. When the oil gap remains unbroken, its impedance approaches infinity, resulting in the applied voltage drop being entirely across the oil gap. M. J. Kushner and colleagues have posited that during the gap discharge process, the arc channel behaves resistively [11], [12]. Upon breakdown, the arc penetrates the oil gap, establishing a conductive pathway, at which point the impedance is significantly reduced, approaching zero. When accounting for the influence of stray capacitance and ground capacitance, the circuit can be equivalently represented as a typical second-order RLC oscillatory circuit. In this model, the transformer is equivalent to an inductor with internal resistance, while the oil gap, traversed by the arc channel, can be modeled as a series configuration of a resistor and a small inductor. The equivalent capacitance reflects the combined effects of stray capacitance and ground capacitance, which elucidates the oscillatory phenomena observed in the pulse current waveforms recorded by the oscilloscope.

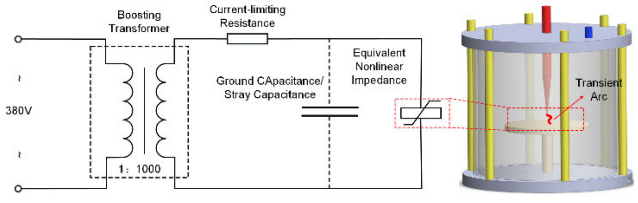


**FIGURE 5.** Equivalent circuit diagram of the test.

In the moment of breakdown, the oil gap is effectively bridged by the arc, resulting in the arc gap resistance, denoted as $Z_{\text{arc}}$. The external circuit can be represented by a Thévenin equivalent circuit comprising a voltage source $U_{\text{s}}$ and an impedance $Z_{\text{in}}$. Once the arc channel is established, the voltage across the oil gap transitions from a value close to the supply voltage to a significantly reduced voltage determined by the arc resistance.

$$U_{arc} = U_S \cdot \frac{Z_{arc}}{Z_{arc} + Z_{in}} \tag{1}$$

Upon the introduction of a current-limiting resistor in the circuit, the impedance $Z_{\text{in}}$ is relatively high. However, once the arc channel within the oil gap becomes conductive, the presence of the plasma channel requires only a minimal voltage to sustain its operation without extinguishing. Consequently, the current will rapidly decrease and ultimately stabilize at the maintenance current $I_{\infty}$:

$$I_{\infty} = \frac{U_S}{Z_{in}} \tag{2}$$

At the moment of breakdown within the oil gap, the resulting surge current $I_{\text{pluse}}$ can be estimated using:

$$I_{\text{pluse}} = C\frac{\Delta U}{\Delta t} \tag{3}$$

where $\Delta U = U_{\text{s}}\text{-}U_{\text{arc}} \approx U_{\text{s}}$. Here, the capacitance referenced here pertains to the stray capacitance of the oil gap, which typically falls within the range of several picofarads (pF). Consequently, the estimated magnitude of the resulting impulse current is approximately:

$$I_{\text{pluse}} = C\lim\frac{\Delta U}{\Delta t} = 3\text{p}F\frac{30\text{k}V}{5\text{ns}} = 18A \tag{4}$$

It is important to clarify that the values presented here are intended for estimating the magnitude of the impulse current and do not necessarily reflect actual conditions. Nevertheless, this estimation aligns with the observations encountered during our experiments. Despite numerous engineering simplifications made throughout the process, the calculated values are consistent with the maximum peak current of 27 A recorded by the oscilloscope at the moment of breakdown, as shown in Figure 6.

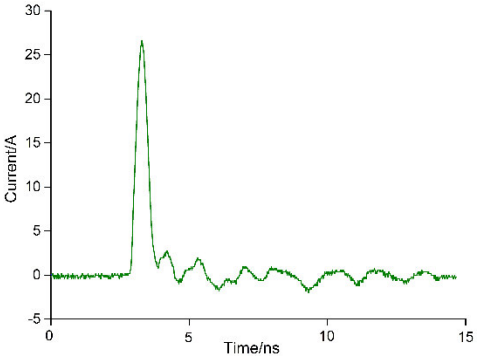


**FIGURE 6.** Transient pulse current in the breakdown test.

The current waveform captured by the oscilloscope also exhibits oscillations, indicating that the actual equivalent circuit is likely a complex higher-order RLC oscillatory circuit. During the decline of the current, two components are present: a rapid decay of the transient impulse current $I_{\text{pulse}}$ and the maintenance current $I_{\infty}$ determined by the external circuit, which results in a relatively prolonged decay time of the pulse current.

### B. ELECTRICAL ABLATION CHARACTERISTICS

The results presented in Figure 7 depict scanning electron microscopy (SEM) images of the ablation holes surrounding 0.05 mm thick copper and silver plates after they have been penetrated. The differences in the ablation characteristics of copper and silver are more pronounced in these images: the surface of the copper exhibits a greater number of holes and voids following arc ablation, whereas the silver electrode's surface displays a higher density of pits resulting from electrical ablation. The observed variations in surface morphology can be attributed to several factors, including the physical properties of the materials and the chemical stability of metal oxides.

During the arc ablation process, the high-temperature plasma generated by the arc impacts the cathode surface, resulting in localized melting and vaporization of the material. Due to silver's lower melting point, it is more susceptible to melting during arc discharge. Coupled with its excellent thermal conductivity, silver efficiently dissipates heat to the surrounding areas, thereby preventing the formation of local hot spot. Furthermore, silver oxides are inherently unstable and tend to decompose under the high temperatures of the arc, making it difficult for unstable oxides to grow and form localized protrusions on the surface, which is the main reason for the difference in surface morphology. These characteristics contribute to the maintenance of a relatively flat and smooth surface on the silver electrode, which in turn enhances the uniformity of discharge and reduces the risk of gap shortening due to protrusions. In contrast, copper, with its higher melting point and relatively stable oxides, is prone to the formation of protrusions and oxides during arc discharge. These features can adversely affect the discharge process and the uniformity of the cathode surface, ultimately diminishing the electrode's lifespan. After arc discharge, the stability of copper oxides complicates their removal, often resulting in the formation of a thick oxide layer on the surface. This oxide layer can act as a barrier to current flow, increasing resistance and leading to localized overheating and further ablation.

Figure 8 presents the EDS analysis of the metal sheets, detailing the elemental mass and atomic percentage composition. The results indicate the presence of oxides following arc ablation, with the oxygen content on the copper surface significantly higher (atomic percentage of 10.74% and mass percentage of 7.75%) compared to that on the silver surface (atomic percentage of 1.07% and mass percentage of 0.42%). Additionally, the percentage of oxygen in the ablated regions of the copper surface exceeds that of the silver surface. This finding corroborates our earlier hypothesis: the stability of copper oxides allows for their adherence and growth on the surface, resulting in the formation of protrusions and irregular morphologies. In contrast, the lower stability of silver oxides leads to their decomposition under the high temperatures of the arc, resulting in a reduced oxygen content on the silver surface and a relatively smoother post-ablation morphology.

### C. MATERIAL TRANSFER PROCESS IN ARC ABLATION

The arc formation process can be delineated into two distinct phases [10], [13], [14], [15]: the metallic arc phase (Phase I) and the gaseous arc phase (Phase II), as illustrated in Figure 9.

During Phase I, following the rupture of the liquid bridge, localized regions on the electrode surface experience elevated temperatures. This thermal effect facilitates the emission of electrons from these high-temperature areas. Concurrently, the minimal inter-electrode spacing generates a substantial electric field, potentially reaching magnitudes of 10^7 V/m, which further promotes electron emission from the cathode surface. Consequently, this localized region on the cathode acts as a thermionic-field emission source. The emitted electrons, accelerated by the electric field, collide inelastically with metal vapor, resulting in ionization and the generation of additional electrons, akin to an electron avalanche, thereby establishing the metallic arc.

As the process transitions into Phase II, characterized by the continued separation of the contacts, the nature of the arc evolves. The density of the metal vapor diminishes over time due to two primary factors: the deposition of metal ions onto the cathode surface and the diffusion of these ions into the surrounding medium (insulating oil), which leads to their gradual elimination. Thus, the insulating oil becomes the predominant medium between the electrodes. When the power supply reaches sufficiently high levels, the insulating oil undergoes ionization, leading to thermal decomposition and the generation of gas. As the concentration of gaseous ions increases, they begin to play a significant role in the arc dynamics, facilitating the transition from a metallic arc to a gaseous arc.

Throughout this process, material transfer occurs from the anode to the cathode during the metallic arc phase,

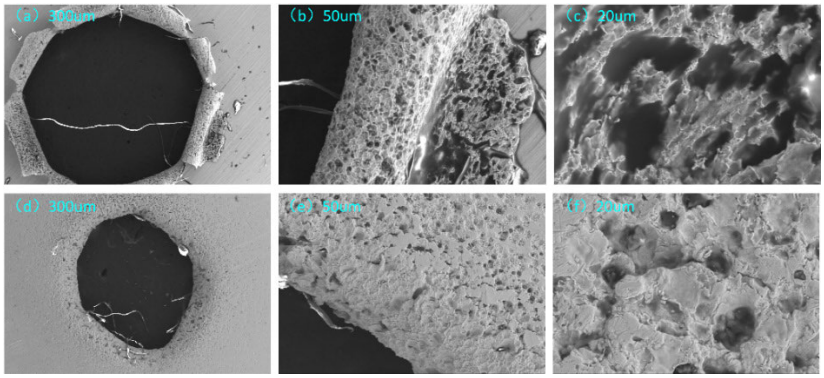


**FIGURE 7.** SEM image of cathode after burn-through. (a)-(c): copper (d)-(f): silver.

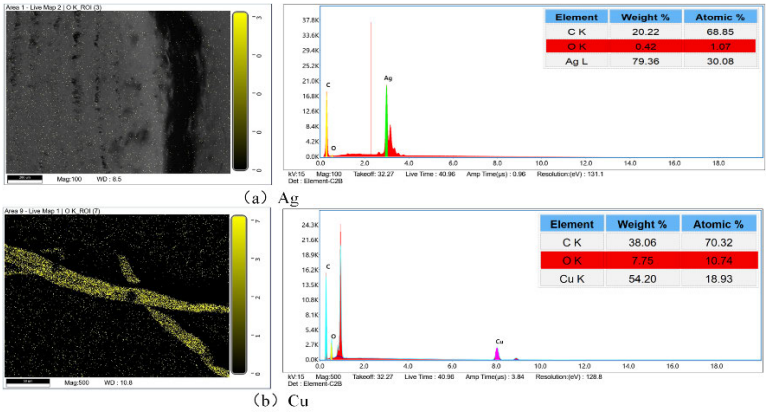


**FIGURE 8.** EDS analysis of cathode after electrical ablation.

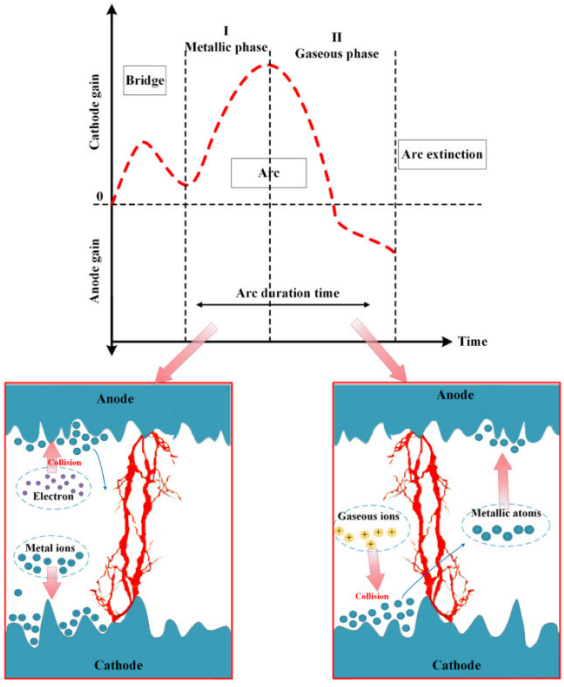


**FIGURE 9.** Schematic diagram of arc erosion process.

resulting in an increase in the mass of the cathode's metallic material. However, as the discharge transitions from the metallic to the gaseous arc, the direction of material transfer reverses, shifting from the cathode to the anode. With the further development of the gaseous arc, both the anode and cathode experience material loss. Under the influence of the arc, metal atoms lose electrons to form ions, while some high-temperature metal particles or ions escape and are subsequently cooled and absorbed by the surrounding insulating oil, leading to an increase in the metal content within the oil. Due to the movement and collision of metal ions between the electrodes in both processes, there is a possibility of escaping metal particles in both stages.

Figure 10 illustrates the internal disassembly of a transformer during major maintenance. The presence of various arc ablation and overheating at solder joints leads to the generation of metallic particles, which subsequently accumulate at the bottom of the oil tank.

## III. THE PROCESS OF METAL CORROSION IN OIL

The corrosion of metals in the oil is fundamentally a chemical erosion process, wherein the transformation of metals into soluble metal ion compounds is a critical step. Previous studies have identified the corrosive sulfide dibenzyl disulfide (DBDS) as a primary contributor to the corrosion of transformer windings [16], [17], [18]. Its chemical reactivity significantly increases at temperatures exceeding 80°C, exacerbating the chemical corrosion effects

**FIGURE 10.** Scene picture: metal particles in the oil.

on contacts that experience abnormal heating. The acidic environment within the insulating oil further enhances the corrosive activity of sulfides. In oil-paper insulation systems, the sources of acidity can be categorized into two main types [19], [20], [21]: one is the high molecular weight acids generated during the acidification and aging of the insulating oil, such as oleic acid (OA); the other is the low molecular weight acids produced from the degradation of the fibrous structure of the insulating paper, such as formic acid (FA). The differing formation mechanisms of these high and low molecular weight acids lead to distinct distributions within the transformer's oil-paper insulation system, which in turn influences the distribution of metal corrosion products within the transformer. This study primarily focuses on elucidating the key factors contributing to the formation of soluble metal ion compounds.

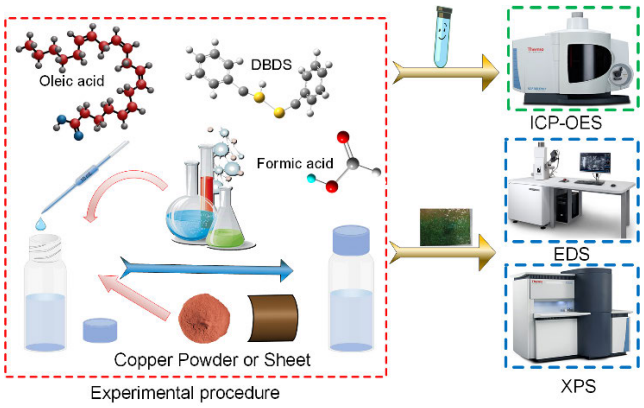


**FIGURE 11.** Schematic diagram of capacitance probe.

The experimental sample preparation and testing procedures are illustrated in Figure 11, which delineates two distinct groups: the copper powder group and the copper sheet group [22]. The copper powder group is designed to expedite the corrosion process, facilitating the observation of overall changes in the liquid medium while concurrently detecting the concentration of metal ions in the oil. In contrast, the copper sheet group is established to facilitate a more detailed analysis of the composition of the corrosion products.

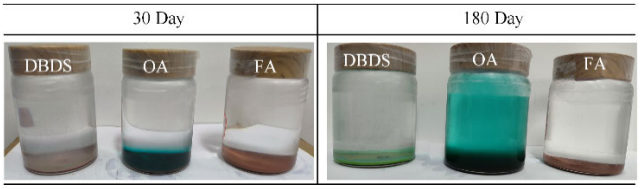


**FIGURE 12.** Schematic diagram of capacitance probe.

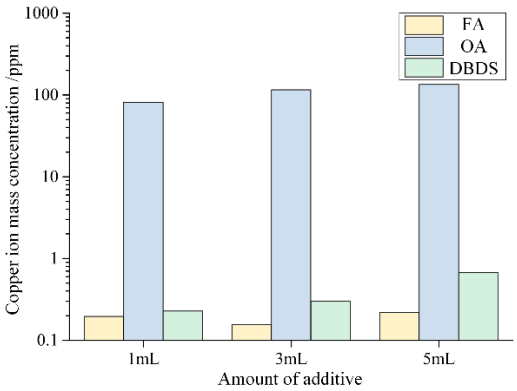


**FIGURE 13.** Comparison of single additive corrosion results.

In this experiment, the concentration of metal ions was quantified using inductively coupled plasma optical emission spectrometry (ICP-OES). Surface elemental analysis was conducted through a combination of energy-dispersive X-ray spectroscopy (EDS) and X-ray photoelectron spectroscopy (XPS) to provide a comprehensive assessment of the material composition. As the samples from the copper powder group were soaked in oil, they gradually settled to the bottom over time due to gravity. It was difficult to thoroughly dry the samples when collecting the corrosion products from the copper powder group (during the drying process, the copper powder samples would easily oxidize and change color, even smoke and start to burn). The SEM/EDS/XPS tests all require completion after drying in a vacuum environment. Considering that copper powder and copper sheet are just two different forms of copper, the corrosion products of copper powder should be consistent with those on the surface of copper sheet. For the convenience of subsequent tests, we remade samples of corroded copper sheets.

### A. CORROSION TEST RESULTS

The corrosion behavior of samples containing copper powder with the addition of DBDS, FA, and OA after 30 and 180 days is presented in Figure 12. The samples with DBDS showed no significant changes in corrosion over both 30 and 180 days. In contrast, for samples with FA, green corrosion products began to appear in localized regions of the copper powder after 30 days, and by 180 days, the entire bottom surface was predominantly covered with these green corrosion products. The samples with OA exhibited more pronounced changes; after 30 days, the overall sediment turned deep blue, and by 180 days, the deep blue regions had expanded to cover the entire solution. This observation suggests that the corrosion

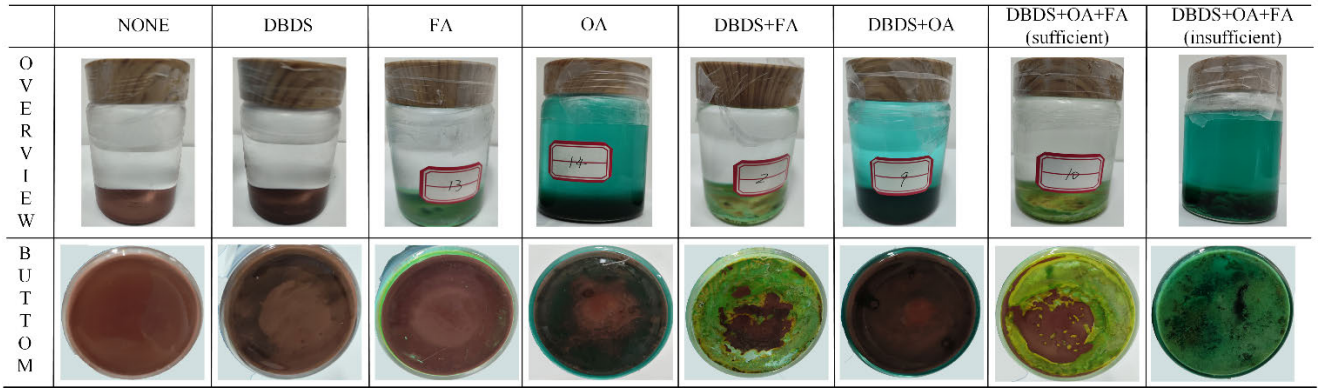


**FIGURE 14.** Comparison of changes in solution and deposition after corrosion in typical samples.

products of copper in the presence of OA are more soluble and can diffuse more effectively in insulating oil compared to those produced by DBDS and FA. Figure 13 presents the mass concentration of copper ions in the solution, further illustrating that the copper ion concentration in samples with DBDS and formic acid was minimal and showed little difference between the two, whereas the copper ion concentration in the oleic acid sample was significantly higher, being hundreds of times greater than that in the other two samples.

Figure 14 summarizes the corrosion processes of typical copper powder samples during the experimental phase, illustrating both the solution and the sedimentation of corrosion products. The figure allows for a comparative analysis of the reaction intensity and the distinct characteristics of the corrosion products. For instance, samples containing DBDS exhibit localized darkening compared to the blank sample, potentially indicating the formation of $Cu_2S$ or $Cu_2O$. In samples with formic acid, blue-green corrosion products are observed in the sediment, aligning with the characteristics of copper formate, although the presence of copper carbonate or copper hydroxide cannot be ruled out. Conversely, copper powder samples treated with oleic acid demonstrate a notable overall color change in the solution, consistent with the characteristics of copper oleate. However, the addition of excess acid results in the disappearance of the characteristic color reaction of copper oleate, suggesting that copper ions from the oleate may react with formic acid to form insoluble copper formate or other insoluble copper compounds.

### B. CORROSION PRODUCT ANALYSIS

Figure 15 presents the EDS surface scan results for copper samples with various additives, illustrating the elemental mass fractions on the surface of different samples. The data indicate that oleic acid significantly corrodes the copper surface, primarily resulting in the formation of soluble copper oleate. Notably, OA does not appear to enhance the sulfur corrosion process, as evidenced by the minimal difference in overall sulfur content between the OA and the OA+DBDS groups. In contrast, when both FA and OA are present, the sulfur content in the surface corrosion products reaches its peak. In regions where corrosion products are markedly accumulated, the sulfur content increases significantly, exceeding 10%.

The results obtained from the EDS area scanning allow for the following conclusions: the addition of oleic acid has a negligible effect on the formation of sulfide corrosion products on the surface, whereas formic acid can significantly accelerate the process of sulfide corrosion. Integrating these findings with the previous measurements of copper ion concentration reveals a distinct difference in the corrosion mechanisms of OA and FA on copper. The interaction between OA and copper predominantly results in the formation of soluble oleic copper, which exhibits favorable solubility and diffusion characteristics in insulating oil. In contrast, the corrosion products associated with FA are primarily characterized by surface growth on the copper substrate (with sedimentation occurring at the bottom in the copper powder samples due to gravitational effects). The simultaneous presence of formic and OA leads to an increased accumulation of surface sulfides, while the concentration of copper ions in the oil diminishes. This suggests that the actual reaction process involves a substantial amount of copper reacting with oleic acid to form soluble copper, which, in the presence of FA, further reacts to generate insoluble formic copper or other copper compounds that subsequently deposit on the surface.

In this experiment, we focus our analysis on the samples associated with oleic acid, specifically examining the corrosion metal surfaces of OA, OA+DBDS, and OA+DBDS+FA. The corrosion products from these samples induced a notable chromatic reaction in the solution, suggesting that the resultant compounds exhibit favorable solubility and diffusivity in the oil medium.

In XPS analysis, peak fitting of high-resolution spectra for different elements is commonly employed to differentiate between the various chemical states of a sample, based on the binding energy differences associated with each state [23], [24], [25], [26]. This approach allows for the identification of potential chemical species present in the sample. Figure 16

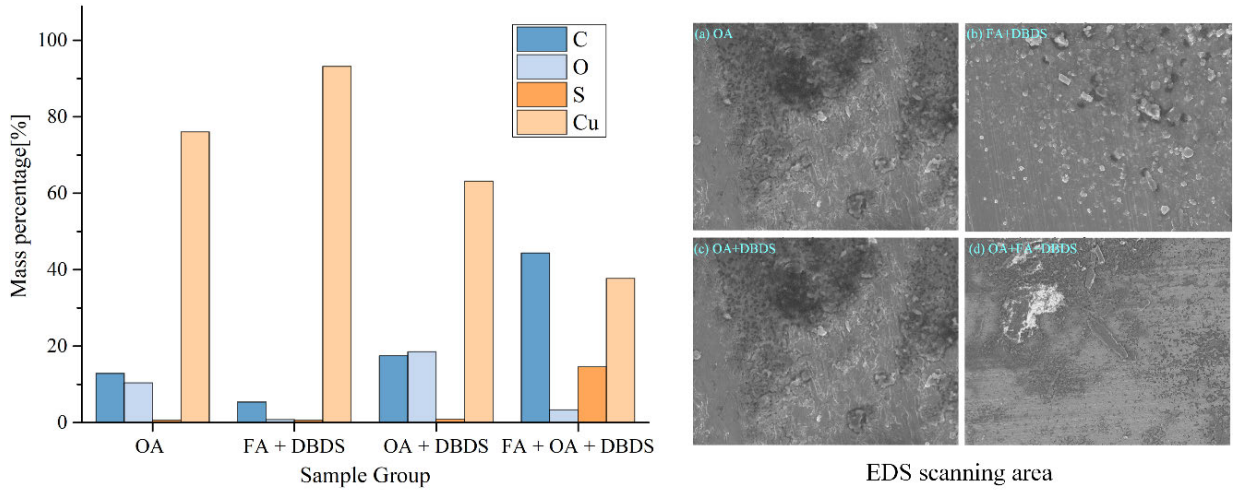


**FIGURE 15.** Comparison of single additive corrosion results.

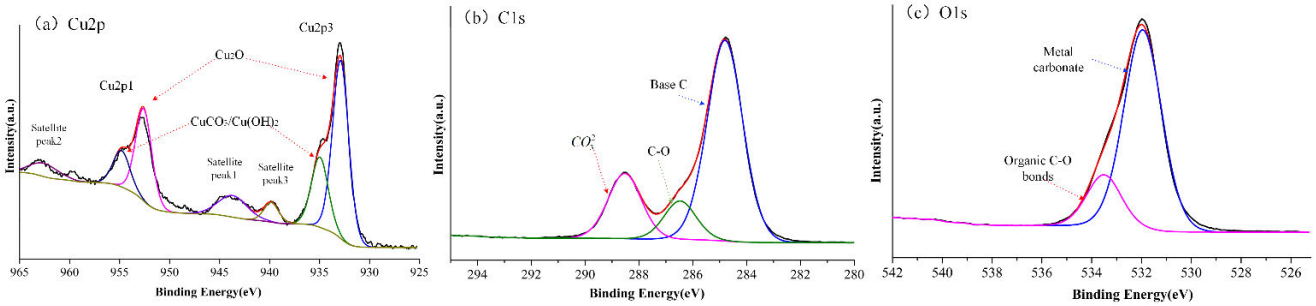


**FIGURE 16.** The fine XPS spectrums of the metal corrosion sample with OA.

displays the high-resolution spectra for C, O, and Cu elements on the surface of the oleic acid-treated corrosion samples, with corresponding peak fittings. In Figure 16(a), the presence of distinct satellite peaks indicates the existence of Cu in the +2 oxidation state, with a binding energy of 932.9 eV (Cu2p3/2) corresponding to Cu2O. The peak near 935 eV (Cu2p3/2) is characteristic of divalent copper. Notably, Cu2O can react with water dissolved in the oil under certain conditions to form Cu(OH)2, suggesting the potential presence of Cu(OH)2 in the sample. The C1s peak at around 289 eV typically signifies the presence of carbonates, confirming the existence of CuCO3 when correlated with the observed color changes during corrosion. The peak at 286.5 eV is attributed to the organic C-O bond, which is indicative of the C-O bond in copper oleate. The O1s peak fitting similarly confirms the presence of organic C-O bonds and metal carbonates. Thus, the corrosion products in the oleic acid-treated samples can be identified as comprising copper carbonate, copper oleate, copper oxide, cuprous oxide, with the possible presence of copper hydroxide.

The XPS full spectrum for samples containing OA and dibutyl disulfide (DBDS) is presented in Figure 17. The incorporation of oleic acid and DBDS did not alter the sulfur content in the surface corrosion products. This observation, in conjunction with the previously noted chromatic phenomena in the solution, suggests that the

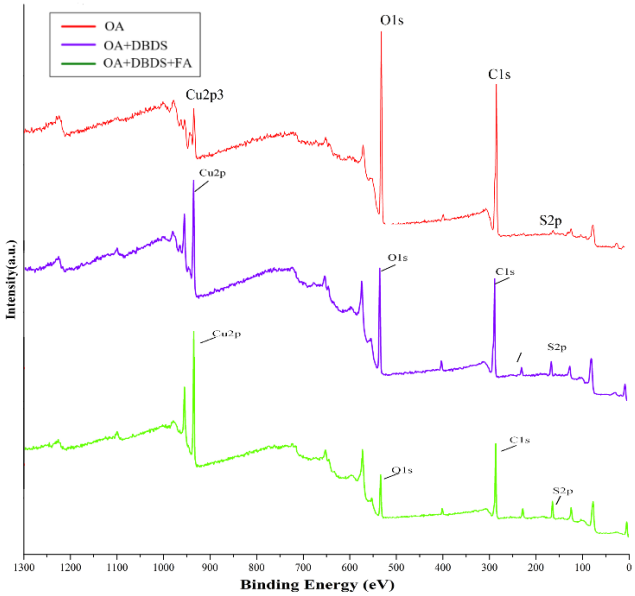


**FIGURE 17.** Comparison of single additive corrosion results.

corrosion products resulting from oleic acid's interaction with copper are soluble oleic acid copper complexes rather than sulfides. While oleic acid exhibits a strong corrosive effect on metallic copper, it does not significantly enhance the

sulfur corrosion process. Analysis of the O fine spectrum reveals a predominant peak at a binding energy of 532 eV, corresponding to the organic C=O double bond, indicating that the oxygen-containing components of the corrosion products are primarily oleic acid copper or copper carbonate. Furthermore, the fine spectrum analysis of sulfur in the OA+DBDS sample indicates the presence of divalent copper and organic C-S-C bonds, suggesting that the involvement of DBDS in the corrosion process leads to the formation of copper compounds containing C-S-C bonds.

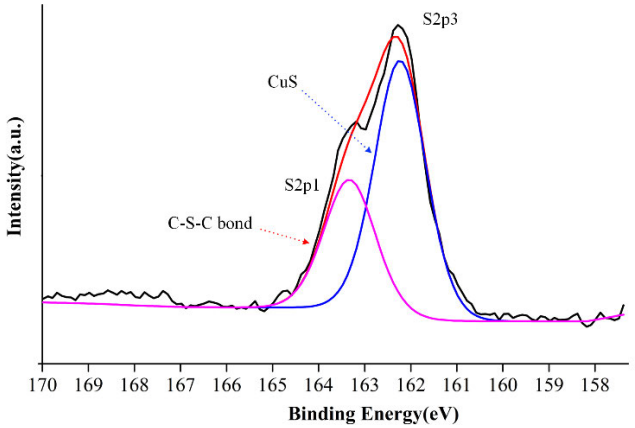


**FIGURE 18.** Comparison of single additive corrosion results.

## IV. CONCLUSION

This study investigates the mechanisms and influencing factors behind the formation of trace metals in oil through electrical ablation and corrosion experiments. The results indicate that the electrical ablation process causes surface damage to metallic materials, leading to the formation of suspended metallic particles in the oil. In contrast, corrosion of metals by aging products of the oil-paper insulation system, particularly high-molecular-weight fatty acids, is identified as the primary cause of the formation of soluble metals in oil. The main conclusions are as follows:

(1) During the electrical ablation process, the arc discharge between contacts leads to material transfer between the metal surfaces, resulting in the loss of metal from the contact surfaces and the formation of suspended metallic particles in the insulating oil. Variations in the stability of oxide films on different materials cause morphological differences in the ablated surfaces, which subsequently affect the uniformity of the discharge process and influence the amount of metal released into the oil.

(2) Oleic acids exhibit strong corrosive effects on copper, with their corrosion products showing high solubility and diffusivity in the oil. As the aging products of insulating oil include high-molecular-weight oleic acids, the corrosive capacity of the oil is expected to increase in the later stages of aging. A synergistic effect between DBDS and acids enhances the corrosion process, predominantly forming insoluble metal sulfides on the surface. However, the formation of soluble copper in the oil is primarily attributed to corrosion by oleic acids.

## REFERENCES

[1] *Transformer Reliability Survey*, CIGRE Tech. Brochure 642, Paris, France, Dec. 2015.

[2] *HVDC Transformer Failure Survey Results From 2013 to 2020*, CIGRE Tech. Brochure 859, Paris, France, Dec. 2021.

[3] F. Vahidi, S. Haegele, S. Tenbohlen, K. Rapp, and A. Sbravati, "Study on moisture influence on electrical conductivity of natural ester fluid and mineral oil," in *Proc. IEEE Electr. Insul. Conf. (EIC)*, Baltimore, MD, USA, Jun. 2017, pp. 290–293, doi: 10.1109/EIC.2017.8004614.

[4] J. Dai, H. Song, G. Sheng, and X. Jiang, "Dissolved gas analysis of insulating oil for power transformer fault diagnosis with deep belief network," *IEEE Trans. Dielectr. Electr. Insul.*, vol. 24, no. 5, pp. 2828–2835, Oct. 2017, doi: 10.1109/TDEI.2017.006727.

[5] M. Badar, P. Lu, Q. Wang, T. Boyer, K. P. Chen, and P. R. Ohodnicki, "Real-time optical fiber-based distributed temperature monitoring of insulation oil-immersed commercial distribution power transformer," *IEEE Sensors J.*, vol. 21, no. 3, pp. 3013–3019, Feb. 2021, doi: 10.1109/JSEN.2020.3024943.

[6] R. M. De Carlo, M. C. Bruzzoniti, C. Sarzanini, R. Maina, and V. Tumiatti, "Copper contaminated insulating mineral oils-testing and investigations," *IEEE Trans. Dielectr. Electr. Insul.*, vol. 20, no. 2, pp. 557–563, Apr. 2013, doi: 10.1109/TDEI.2013.6508759.

[7] K. Wang, F. Wang, J. Li, Q. Zhao, G. Wen, and T. Zhang, "Effect of metal particles on the electrical properties of mineral and natural ester oils," *IEEE Trans. Dielectr. Electr. Insul.*, vol. 25, no. 5, pp. 1621–1627, Oct. 2018.

[8] Y. X. Zhou, Y. L. Xue, and K. Zhou, "Failure analysis of arc ablated tungsten-copper electrical contacts," *Vacuum*, vol. 164, pp. 390–395, Jun. 2019.

[9] W. Guan, J. Yuan, H. Lv, T. Zhu, Y. Fang, J. Liu, H. Wang, Z. Li, Z. Tang, and W. Yang, "Homogeneous arc ablation behaviors of CuCr cathodes improved by chromic oxide," *J. Mater. Sci. Technol.*, vol. 81, pp. 1–12, Aug. 2021.

[10] K. Liang, F. Wang, L. Zhong, S. Chen, Q. Sun, X. Duan, and S. Liu, "Arc ablation on metal contact in insulating oil: Microscopic mechanism and influencing factor," *IEEE Trans. Dielectr. Electr. Insul.*, vol. 31, no. 2, pp. 747–755, Apr. 2024, doi: 10.1109/TDEI.2023.3316148.

[11] M. J. Kushner, W. D. Kimura, and S. R. Byron, "Arc resistance of laser-triggered spark gaps," *J. Appl. Phys.*, vol. 58, no. 5, pp. 1744–1751, Sep. 1985.

[12] J. P. VanDevender, "The resistive phase of a high-voltage water spark," *J. Appl. Phys.*, vol. 49, no. 5, pp. 2616–2620, May 1978.

[13] A. Li, W. Zhou, M. Xie, S. Wang, S. Wang, Y. Yang, Y. Chen, and M. Liu, "Preparation and arc erosion behavior of AgNi10 contact material with different allotropes of carbon addition," *Diamond Rel. Mater.*, vol. 111, Jan. 2021, Art. no. 108141.

[14] Z.-K. Chen and K. Sawa, "Effect of arc behavior on material transfer: A review," in *Proc. 42nd IEEE Holm Conf. Electr. Contacts. Joint 18th Int. Conf. Electr. Contacts*, Sep. 1996, pp. 238–251.

[15] P. Kah, R. Suoranta, and J. Martikainen, "Advanced gas metal arc welding processes," *Int. J. Adv. Manuf. Technol.*, vol. 67, pp. 655–674, Jul. 2013.

[16] S. Gao, L. Yang, B. Deng, and J. Zhang, "Corrosion mechanism for local enrichment of acids and copper ions in copper-insulating paper contacts leading to the acceleration of copper sulfide formation induced by dibenzyl disulfide," *RSC Adv.*, vol. 7, no. 83, pp. 52475–52485, 2017.

[17] L. Yang, S. Gao, B. Deng, and Z. Cheng, "Corrosion mechanisms for electrical fields leading to the acceleration of copper sulfide deposition on insulation windings," *Ind. Eng. Chem. Res.*, vol. 56, no. 32, pp. 9124–9134, Aug. 2017.

[18] L.-J. Yang, S.-H. Gao, B.-F. Deng, J. Tang, and J.-J. Huang, "Effects of electric fields on copper sulfide deposition and the properties of insulating oils in oil-immersed transformers," *IEEE Trans. Dielectr. Electr. Insul.*, vol. 24, no. 5, pp. 2847–2853, Oct. 2017.

[19] L. Lundgaard, W. Hansen, and S. Ingebrigtsen, "Ageing of mineral oil impregnated cellulose by acid catalysis," *IEEE Trans. Dielectr. Electr. Insul.*, vol. 15, no. 2, pp. 540–546, Apr. 2008.

[20] L. E. Lundgaard, W. Hansen, S. Ingebrigtsen, D. Linhjell, and M. Dahlund, "Aging of Kraft paper by acid catalyzed hydrolysis," in *Proc. IEEE Int. Conf. Dielectric Liquids*, Jun. 2005, pp. 375–378.

[21] W. Yao, J. Li, Z. Huang, X. Li, and C. Xiang, "Acids generated and influence on electrical lifetime of natural ester impregnated paper insulation," *IEEE Trans. Dielectr. Electr. Insul.*, vol. 25, no. 5, pp. 1904–1914, Oct. 2018.
[22] K. Liang, F. Wang, L. Zhong, S. Chen, Q. Sun, C. Hu, and X. Chang, "Investigation into the formation mechanisms of soluble copper ions in oil: Reconsidering the impact of corrosive sulfides and acids," *IEEE Trans. Dielectr. Electr. Insul.*, vol. 31, no. 2, pp. 683–693, Apr. 2024, doi: 10.1109/TDEI.2024.3370131.
[23] M. C. Biesinger, "Accessing the robustness of adventitious carbon for charge referencing (correction) purposes in XPS analysis: Insights from a multi-user facility data review," *Appl. Surf. Sci.*, vol. 597, Sep. 2022, Art. no. 153681.
[24] M. A. Fazal, A. S. M. A. Haseeb, and H. H. Masjuki, "Corrosion mechanism of copper in palm biodiesel," *Corrosion Sci.*, vol. 67, pp. 50–59, Feb. 2013.
[25] H. Nohira, W. Tsai, W. Besling, E. Young, J. Petry, T. Conard, W. Vandervorst, S. De Gendt, M. Heyns, J. Maes, and M. Tuominen, "Characterization of ALCVD-$Al_2O_3$ and $ZrO_2$ layer using X-ray photoelectron spectroscopy," *J. Non-Crystalline Solids*, vol. 303, no. 1, pp. 83–87, May 2002.
[26] A. Shchukarev and D. Korolkov, "XPS study of group IA carbonates," *Open Chem.*, vol. 2, no. 2, pp. 347–362, Jun. 2004.

**FENG WANG** (Senior Member, IEEE) was born in Liaoning, China, in 1972. He received the B.Sc. and Ph.D. degrees in electrical engineering from Xi'an Jiaotong University, Xi'an, China, in 1994 and 2003, respectively.

He is currently a Professor with the College of Electronic and Information Engineering, Yili Normal University, and the College of Electrical and Information Engineering, Hunan University, Changsha, China. His research interests include electric arc and intelligent monitoring and diagnosis of power systems.

**HUIMIN ZHANG** was born in Shandong, China, in 2001. She received the bachelor's degree in electronic and information engineering from Yili Normal University, in 2023, where she is currently pursuing the master's degree in radio physics with the Department of Electronics and Engineering.

Her research interests include signal and information processing and its application in power equipment and surface discharge dissipation techniques.

**HAOCHENG WANG** was born in Xinjiang, China, in 1992. He received the B.Sc. degree in wind energy and power engineering from Xinjiang University, Urumqi, China, and the M.Sc. degree in electrical engineering, in 2020.

He is currently a Lecturer with the College of Electronics and Information Engineering, Yili Normal University, China. His current research interests include grid-connected converter control and the stability control of renewable energy power generation systems.

**DILIXIATI HAYIREDING** received the B.E. degree in wind energy and power engineering and the M.E. degree in renewable energy science engineering from Hohai University, Nanjing, China, in 2014 and 2017, respectively. He is currently pursuing the Ph.D. degree in electronic information engineering with Anhui University, Hefei, China.

Since 2017, he has been with the School of Electronics and Engineering, Yili Normal University, as a Lecturer. His research interest includes signal and information processing and its application in power systems.

**CANGUAN GAO** was born in 1975. He received the Ph.D. degree in space microwave remote sensing systems from the Chinese Academy of Sciences, Beijing, China. He is currently a Professor with the Department of Electronics and Engineering, Yili Normal University. His research interest includes space microwave technology.

**GUOLIANG ZHANG** was born in 1967. He received the B.Sc. degree in space microwave from Yunnan University, Kunming, China. He is currently a Professor with the Department of Electronics and Engineering, Yili Normal University. His research interest includes space microwave technology.

**KAIBIN LIANG** was born in Hunan, China, in 1990. He received the B.Sc. and M.Sc. degrees in electrical engineering from the School of Electrical Engineering, Wuhan University, Wuhan, China, in 2012 and 2016, respectively, and the Ph.D. degree in electrical engineering, in 2023. He was with PetroChina, in 2013, and State Grid, from 2016 to 2019. He continued his work as a Postdoctoral Researcher at Hunan University, Changsha, China. His research interests include power equipment intelligent monitoring and diagnosis, and surface discharge dissipation technique.

**HENG YI** was born in Hunan, China, in 1997. He received the B.S. and M.S. degrees from North China Electric Power University, China, in 2020 and 2023, respectively. He is currently pursuing the Ph.D. degree with Hunan University, Changsha, China. His research interests include online monitoring of power equipment and surface discharge dissipation techniques.

**ZEPING HUANG** was born in Fujian, China, in 1997. He received the B.S. and M.S. degrees from Xiamen University of Technology, China, in 2020 and 2023, respectively. He is currently pursuing the Ph.D. degree with Hunan University, Changsha, China. His research interests include air discharge, high-voltage insulation, and online monitoring of power equipment.

**CHANGHAO HU** was born in Guangxi, China, in 1998. He received the B.E. degree in electrical engineering from Hunan University, in 2021, where he is currently pursuing the M.Sc. degree in electrical engineering. His research interests include high-voltage and insulation technology.